

# Electronic Structure and Optical Properties of CsPbF<sub>3-y</sub>I<sub>y</sub> ( $y = 0, 1, 2$ ) Cubic Perovskites

A. AMUDHAVALLI<sup>a</sup>, R. RAJESWARAPALANICHAMY<sup>a,\*</sup>,  
R. PADMAVATHY<sup>a</sup> AND K. IYAKUTTI<sup>b</sup>

<sup>a</sup>Department of Physics, N.M.S.S. Vellaichamy Nadar College, Madurai-625019, India

<sup>b</sup>Department of Physics and Nanotechnology, SRM Institute of Science and Technology, SRM Nagar, Kattankulathur, Chennai, Tamilnadu-603203, India

Received: 27.01.2021 & Accepted: 18.03.2021

Doi: [10.12693/APhysPolA.139.692](https://doi.org/10.12693/APhysPolA.139.692)

\*e-mail: [rrpalanichamy@gmail.com](mailto:rrpalanichamy@gmail.com)

The structural property, electronic structure and optical properties of lead-based halide perovskites CsPbF<sub>3-y</sub>I<sub>y</sub> ( $y = 0, 1, 2$ ) are investigated. The computed electronic structure profile of CsPbF<sub>3-y</sub>I<sub>y</sub> ( $y = 0, 1, 2$ ) reveals that these materials exhibit semiconducting behavior at normal pressure. The energy gap of CsPbF<sub>3</sub> is tuned by substituting iodine atoms for fluorine atoms. The optical parameters, such as dielectric function, electron energy loss function, refractive index and reflectivity, are computed. The optical properties of these lead-based halide perovskites against the incident photon energy radiation indicate that these materials can be effective candidates for the solar cell applications.

topics: semiconductors, *ab initio* calculations, electronic structure, optical properties

## 1. Introduction

Metal halide perovskite solar cells are rapidly becoming increasingly competitive with conventional photovoltaic technologies. The power conversion efficiency is increased from 3.8% to 22% after the invention of perovskite-based solar cells [1]. The impact of tuning the size of the A cation in ABX<sub>3</sub> methylammonium lead triiodide, in changing the band gap of perovskite absorber, was investigated [2]. It was found that the increase in cation size reduces the band gap. Experimentally, lattice constant values of CsPbI<sub>3</sub> and CsPbF<sub>3</sub> were determined as 6.2894 Å and 4.7748 Å [3, 4]. Theoretically, the electronic properties of lead halide perovskites were investigated by first principles calculations based on density functional theory [5–11]. It was observed that the lattice constant was increased when the halide ion changed from Cl to I in CsPbM<sub>3</sub> (M = Cl, Br, I) [8]. The band gap value of CsPbF<sub>3</sub> was computed as 2.55 eV [9]. The band gap values of CsPbX<sub>3</sub> (X = Cl, Br, I) were computed by Chang and Park [10] as 1.97 eV, 1.42 eV and 1.33 eV, respectively, using electronic structure calculation.

In mixed I/Br perovskites ABX<sub>3-x</sub>Br<sub>x</sub>, Noh et al. [11] found that the band gap  $E_g$  can be tuned by changing the halide composition. Several hypotheses explained the variation of the band gap in halide perovskites by the substitution method [12]. Wang et al. [13] obtained highly

crystalline  $\beta$ -CsPbI<sub>3</sub> films with an extended spectral response and enhanced phase stability. The surface passivated, Ba-doped  $\alpha$ -CsPbI<sub>3</sub> was found to be thermally stable [14]. A general approach for deposition of  $\gamma$ -CsPbI<sub>3</sub> films at 100 °C with high photoluminescence quantum efficiencies by adding organic ammonium cations was demonstrated and it was found that the light-emitting diode exhibited an external quantum efficiency of 10.4% with suppressed efficiency roll-off [15]. The limitations of tolerance factors in predicting perovskite stability were analyzed and the detailed structural information suggested the methods to engineer stable CsPbI<sub>3</sub>-based solar cells [16]. Using first principles calculations, Roma et al. [17] showed that the alkali lead halides, CsPbI<sub>3</sub>, CsPbCl<sub>3</sub>, CsPbBr<sub>3</sub> and CsPbF<sub>3</sub> have collective ferroelectric polarization. A novel class of sensitive filterless narrowband near-infrared photodetectors (NIRPDs) in CsPbF<sub>3</sub>:Zn<sup>2+</sup>-Yb<sup>3+</sup>-Tm<sup>3+</sup> (or Er<sup>3+</sup>) perovskite nanocrystals were investigated both theoretically and experimentally [18]. First-principles DFT calculations have shown that pressure directs the out-of-phase and in-phase octahedral tilts that control the relative energy difference between the competing  $\delta$ - and  $\gamma$ -CsPbI<sub>3</sub> and ultimately stabilizes  $\gamma$ -CsPbI<sub>3</sub> [19].

In our previous work, the electronic structure and optical properties of CsPbBr<sub>3-y</sub>I<sub>y</sub> ( $y = 0, 1, 2, 3$ ) were analyzed [20]. Tuning the band gap of CsPbF<sub>3</sub> by the substitution of the halide atom iodine (I)

TABLE I

Calculated equilibrium volume  $V_0$  [ $\text{\AA}^3$ ], lattice parameter  $a$  [ $\text{\AA}$ ], valence electron density  $\rho$  [electrons/ $\text{\AA}^3$ ], formation enthalpy  $\Delta H$  [eV], bulk modulus  $B_0$  [GPa], its derivative  $B'_0$  and energy gap  $E_g$  [eV] for  $\text{CsPbF}_3$ ,  $\text{CsPbF}_2\text{I}$ ,  $\text{CsPbFI}_2$ , and  $\text{CsPbI}_3$ . Experimental results ([4], [6], [7]) and the theoretical ones ([5], [8], [9], [10], [13]) are shown for comparison.

Compound	$V_0$ [ $\text{\AA}^3$ ]	$a$ [ $\text{\AA}$ ]	$\rho$ [electrons/ $\text{\AA}^3$ ]	$\Delta H$ [eV]	$B_0$ [GPa]	$B'_0$ [GPa]	$E_g$ [eV]	
							GGA	HSE06
$\text{CsPbF}_3$	116.02	4.8773	0.2585	-1.82	39.035	5.765	2.642	3.707
	108.864 <sup>a</sup>	4.7748 <sup>a</sup>					2.55 <sup>c</sup>	
	109.041 <sup>b</sup>	4.777 <sup>b</sup>						
$\text{CsPbF}_2\text{I}$	186.71	5.7155	0.1606	-1.51	27.948	5.684	1.674	2.855
$\text{CsPbFI}_2$	227.56	6.1052	0.1318	-1.27	18.291	5.403	1.477	2.307
$\text{CsPbI}_3$	259.96 <sup>d</sup>	6.3822 <sup>d</sup>	0.1154 <sup>d</sup>	-1.16 <sup>d</sup>	12.495 <sup>d</sup>	5.468 <sup>d</sup>	1.307 <sup>d</sup>	2.030
	259.998 <sup>e</sup>	6.3824 <sup>e</sup>					1.478 <sup>e</sup>	
		6.383 <sup>g</sup>					1.359 <sup>g</sup>	
		6.18 <sup>f</sup> , 6.05 <sup>h</sup>					1.3 <sup>f</sup> , 1.33 <sup>h</sup>	

<sup>a</sup>Ref. [4], <sup>b</sup>Ref. [7], <sup>c</sup>Ref. [9], <sup>d</sup>Ref. [13], <sup>e</sup>Ref. [6], <sup>f</sup>Ref. [8], <sup>g</sup>Ref. [5], <sup>h</sup>Ref. [10]

is not yet reported. In this work, the electronic structure calculation is performed to tune the band gap of  $\text{CsPbF}_3$  and optical properties of  $\text{CsPbF}_{3-y}\text{I}_y$  ( $y = 0, 1, 2$ ) are analyzed.

## 2. Computational details

The total energy calculation is performed using VASP code (Vienna *ab initio* simulation package) based on density functional theory (DFT) [21–25]. The interaction between ions is described by the projector augmented wave method. The Kohn–Sham equations are solved self-consistently to obtain total energies. The exchange and correlation are treated by generalized gradient approximation (GGA) [26]. A plane wave kinetic energy cut off of 500 eV is used. To compute total energy, the Monkhorst–Pack [27]  $6 \times 6 \times 6$   $k$ -mesh is used for the Brillouin zone integration and is further increased to  $11 \times 11 \times 11$   $k$ -mesh to compute the density of states (DOS) and optical properties. The lattice parameters were fully optimized to residual forces on every atom below  $10^{-5}$  eV employing the conjugate-gradient algorithm. The tetrahedron method of the Brillouin zone integration is adopted to compute the electronic structure [28]. The hybrid density functional is also employed to find the accurate energy gap.

The simplest possible halide perovskite is  $\text{CsPbX}_3$ , which has a high-symmetry cubic structure with the space group  $Pm\bar{3}m$  (221). The lattice positions of Cs, Pb and X atoms are (0, 0, 0), (0.5, 0.5, 0.5) and (0, 0.5, 0.5), respectively. The valence electron configurations are Cs  $6s^1$ , Pb  $6p^2$ , Cl  $3s^2 3p^5$  and F  $2s^2 2p^5$  atoms. The cubic crystal structure for Pb-based perovskites  $\text{CsPbX}_3$  ( $X = \text{F}, \text{I}$ ) with space group  $Pm\bar{3}m$  is shown in Fig. 1.

## 3. Results and discussion

### 3.1. Structural properties

The structural optimization is performed by computing the total energy for various volumes for these Pb-based halide perovskites  $\text{CsPbF}_{3-y}\text{I}_y$  ( $y = 0, 1, 2, 3$ ). The equilibrium lattice constants are obtained. These total energies are then fitted to the Birch–Murnaghan equation of state to compute the bulk modulus  $B$  [29]. The ground state parameters, such as cell volume  $V$  [ $\text{\AA}^3$ ], lattice constant  $a$  [ $\text{\AA}$ ], total energy  $E$  [eV], valence electron density  $\rho$  [electrons/ $\text{\AA}^3$ ], formation enthalpy  $\Delta H$  [J K/mol], bulk modulus  $B_0$  [GPa] and its derivative of  $\text{CsPbF}_{3-y}\text{I}_y$  ( $X = \text{Br}, \text{Cl}, \text{F}$ ), ( $y = 0, 1, 2$ ) perovskites are listed in Table I along with the experimental and other theoretical values [4–10, 20] for comparison. One can see there, that lattice constant  $a$  and the cell volume  $V$  are comparable to the other results [5, 6]. The lattice constant value of  $\text{CsPbI}_3$  is in good agreement with Ye et al. [5] and Ahmad et al. [6]. The calculated negative formation enthalpy values confirm the thermodynamical stability of these Pb-based perovskites in ideal cubic  $Pm\bar{3}m$  structure.

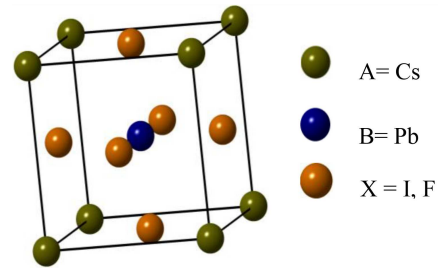


Fig. 1. Crystal structure of the space group ( $Pm\bar{3}m$ ) for  $\text{CsPbX}_3$  ( $X = \text{F}, \text{I}$ ) perovskites.

It is also observed that lattice constant value of  $\text{CsPbF}_3$  is increased when fluorine (F) atom is substituted by iodine (I) atom. This behavior is attributed to the large ionic radius of I compared to the other accompanying halide element F of these  $\text{CsPbF}_{3-y}\text{I}_y$  compounds.

### 3.2. Electronic structure

The electronic structure of  $\text{CsPbF}_{3-y}\text{I}_y$  ( $y = 0, 1, 2$ ) is investigated by computing the total density of states (TDOS) and partial density of states (PDOS) at normal pressure, which are depicted in Fig. 2 and Fig. 3, respectively. It is seen that the valence and conduction states are separated by an energy gap of 2.702 eV for  $\text{CsPbF}_3$ . It is observed that when one atom of iodine is substituted, the energy gap value is decreased from 2.702 eV ( $\text{CsPbF}_3$ ) to 1.674 eV ( $\text{CsPbF}_2\text{I}$ ) and 1.477 eV ( $\text{CsPbFI}_2$ ) when two atoms of iodine are substituted. In general, GGA underestimates the band gap values. Hence, HSE06 functional is employed to compute an accurate energy gap. The computed energy gap values with GGA and HSE06 functional are given in Table I. The energy gap value of  $\text{CsPbF}_3$  is comparable to the result of Qian et al. [9] and the energy gap value of  $\text{CsPbI}_3$  is in good agreement with the result of Murtaza and Ahmad [8]. In Fig. 3, the first peak near  $\sim 20$  eV is due to the Cs 6s state, while the second peak in the valence state ranging from  $-10$  to 0 eV (VB) and the third peak in the conduction state are due to the  $p$ -states of Pb and other halides. The peak around the Fermi level is entirely due to the interaction of  $p$ -states of Pb and  $s$  and  $p$  states of halide atom F.

From the partial density of states (PDOS), it is clear that  $s$  and  $p$  states of Pb and  $p$  state of the halogens play a major role in the reduction of the band gap. The bigger atomic size of iodine (I) contains more nucleons when compared to the smaller F atom. Hence, the larger atomic size of

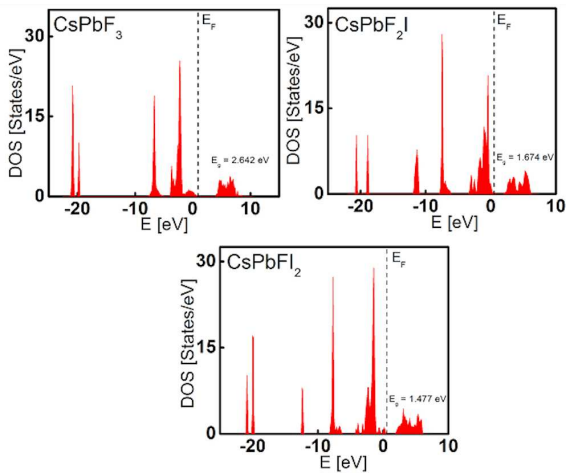


Fig. 2. Total density of states (DOS) for  $\text{CsPbF}_3$ ,  $\text{CsPbF}_2\text{I}$ , and  $\text{CsPbFI}_2$  at normal pressure.

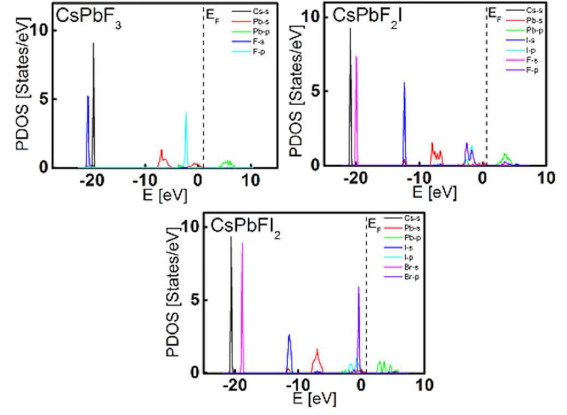


Fig. 3. Partial density of states (PDOS) for  $\text{CsPbF}_3$ ,  $\text{CsPbF}_2\text{I}$ , and  $\text{CsPbFI}_2$  at normal pressure.

the iodine atom causes a decrease in the electrostatic attractive force between the nucleus and the outermost shell electrons and this has reduced the hold of the nucleus on the outermost shell electrons, which lowers the bonding energy and separation between conduction states and valence states. Moreover, the valence state shifts up towards the Fermi level due to the occupation of electrons in the position near the Fermi level, leading to a decrease in the energy gap.

### 3.3. Optical properties

The optical properties of Pb-based semiconducting perovskites are very important to investigate their use in photovoltaic devices. The dielectric function,

$$\varepsilon(\omega) = \varepsilon_1(\omega) + i\varepsilon_2(\omega), \quad (1)$$

describes the optical response of the semiconducting material against the applied field. The imaginary component  $\varepsilon_2(\omega)$  indicates the absorptive behavior. The real component  $\varepsilon_1(\omega)$  is deduced from the imaginary component. The imaginary and real components of the frequency-dependent dielectric function have been calculated using the Kramers–Kronig relations [30, 31]. The real and imaginary components of the dielectric function of these  $\text{CsPbF}_3$ ,  $\text{CsPbF}_2\text{I}$  and  $\text{CsPbFI}_2$  perovskites versus photon energy in the range 0 to 40 eV are shown in Fig. 4.

For  $\text{CsPbF}_3$ ,  $\text{CsPbF}_2\text{I}$  and  $\text{CsPbFI}_2$ , four peaks are mainly observed from the real part of the dielectric function. These four main peaks originate from the electronic transitions from F 2p, Pb 6s in the valence band to the Pb 6p state in the conduction band and other remaining peaks are due to the transition from Cs 6s, F 2p, Pb 6s in the valence band to Cs 5d and 4f in the conduction band [32]. Usually, the imaginary component of the dielectric function is related to the absorption of light. Thus, a prominent peak in the infrared region refers to a strong interaction or absorption between the corresponding lattice vibration and the applied field of

TABLE II

Calculated frequency independent and dependent dielectric constant  $\varepsilon(0)$ ,  $\varepsilon(\omega)$  refractive index  $n(0)$ ,  $n(\omega)$ , and reflectivity  $R(0)$ ,  $R(\omega)$ , and plasma frequency  $\omega_p$  of Pb-based perovskites —  $\text{CsPbF}_3$ ,  $\text{CsPbF}_2\text{I}$ ,  $\text{CsPbFI}_2$ , and  $\text{CsPbI}_3$ . Theoretical results [9] and [11] are shown for comparison.

Compound	$\varepsilon(0)$	$n(0)$	$R(0)$	$\varepsilon(\omega)$	$n(\omega)$	$R(\omega)$	$\omega_p$
$\text{CsPbF}_3$	2.8865	2.3684	0.2589	15.8	3.054	1.28	10.676
	2.707 <sup>a</sup>	1.645 <sup>a</sup>	0.595 <sup>a</sup>				
$\text{CsPbF}_2\text{I}$	2.9038	1.7040	0.2603	17.2	2.282	0.55	11.114
$\text{CsPbFI}_2$	3.0112	1.7353	0.5014	16.4	2.135	0.75	10.443
$\text{CsPbI}_3$	5.4884	2.3427	0.6917	18.9	3.591	0.61	13.093
	6.003 <sup>b</sup>	2.450 <sup>b</sup>	0.177 <sup>b</sup>				

<sup>a</sup>Ref. [9], <sup>b</sup>Ref. [11]

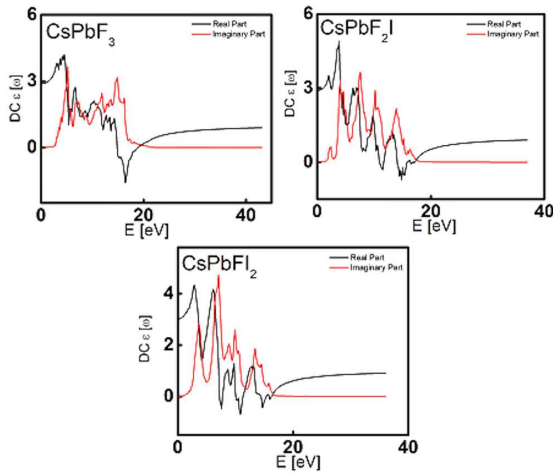


Fig. 4. Energy versus dielectric function of  $\text{CsPbF}_3$ ,  $\text{CsPbF}_2\text{I}$ , and  $\text{CsPbFI}_2$ .

the materials. For  $\text{CsPbF}_3$ ,  $\text{CsPbF}_2\text{I}$ , and  $\text{CsPbFI}_2$ , the threshold energy of imaginary component  $\varepsilon_2(\omega)$  starts around 0.25 eV thereby they attain the prominent peaks at 5.19 eV, 4.12 eV, and 3.69 eV, respectively. The occurrence of the threshold energy is due to the fundamental absorption edge (i.e., the optical transition between the highest valence and lowest conduction bands).

Beyond the threshold energies, the curve of imaginary part  $\varepsilon_2(\omega)$  increases rapidly. The existence of several peaks in imaginary component  $\varepsilon_2(\omega)$  refers to the band to band transition. There is a strong reflection in this range of transition energies. The main peaks of real component  $\varepsilon_1(\omega)$  are situated at 4.53 eV, 3.78 eV, and 2.93 eV for  $\text{CsPbF}_3$ ,  $\text{CsPbF}_2\text{I}$ , and  $\text{CsPbFI}_2$ , respectively, and then there is a decrease with an increase in photon energy. The static dielectric function reveals information about the electronic polarizability of perovskite materials. The static dielectric constant  $\varepsilon_1(0)$  at zero frequency limits of  $\text{CsPbF}_3$ ,  $\text{CsPbF}_2\text{I}$ ,  $\text{CsPbFI}_2$ , and  $\text{CsPbI}_3$  are 2.8865, 2.9038 and 3.0112, respectively. Further beyond the zero limits, it starts increasing and reaches the maximum value of 4.166 at 4.49 eV

for  $\text{CsPbF}_3$ , 4.865 at 3.92 eV for  $\text{CsPbF}_2\text{I}$ , and 4.296 at 2.84 eV for  $\text{CsPbFI}_2$  and goes below zero in the negative region for the energy ranges of 14.92–18.82 eV, 10.95–17.08 eV, and 10.15–11.24 eV of  $\text{CsPbF}_3$ ,  $\text{CsPbF}_2\text{I}$ , and  $\text{CsPbFI}_2$ . In this negative energy region, the real part of the dielectric function  $\varepsilon_1(\omega)$  shows the metallic behavior and other non-negative region represents the dielectric behavior [32]. The peaks in the real part of the dielectric function are found to shift towards the lower energy region which indicates that the incident photons are totally reflected in these regions.

The computed dielectric constant  $\varepsilon(\omega)$  and plasma frequency ( $\omega_p$ ) values are given in Table II. It is observed that these Pb-based semiconducting perovskites fall in the UV range and these materials can be good candidates for UV photodetectors, UV light emitters and power electronic applications due to their fundamental absorption limits and the highest absorption peaks. Another important optical constant is the electron energy loss function  $L(\omega)$ , which is an important parameter describing the inadaptable scattering of highly accelerated electrons passing through the material, characterizing the plasma frequency  $\omega_p$  associated with it. The energy loss function peak represents the combined nature of plasma resonance as well as their related frequency known as plasma frequency  $\omega_p$  above which the material acts as dielectric and below which it shows metallic nature. The electron energy loss functions for  $\text{CsPbF}_3$ ,  $\text{CsPbF}_2\text{I}$ , and  $\text{CsPbFI}_2$  are presented in Fig. 5. The highest energy loss function for all the subjected compounds occurs in the ultraviolet region. It is well known that these peaks are due to interband transitions between various high symmetry points. For  $\text{CsPbF}_3$ ,  $\text{CsPbF}_2\text{I}$ , and  $\text{CsPbFI}_2$ , sharp peaks are found at 18.97, 17.30, and 16.54 eV and the corresponding energy loss function values are 6.20, 7.74, and 7.48 eV, respectively.

Meanwhile, it is worth mentioning that these perovskite compounds could be a good absorber of low and medium UV spectrum, as observed in Fig. 5. The calculated refractive index and reflectivity of semiconducting perovskites have been presented

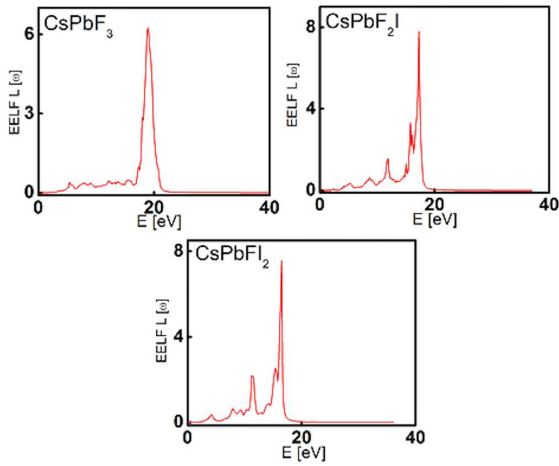


Fig. 5. Energy versus electron energy loss function of CsPbF<sub>3</sub>, CsPbF<sub>2</sub>I, and CsPbFI<sub>2</sub>.

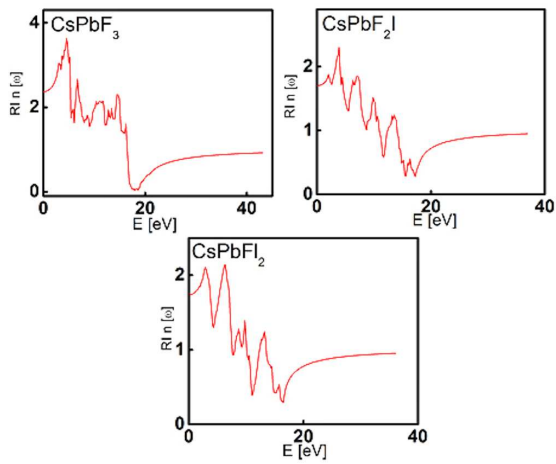


Fig. 6. Energy versus refractive index of CsPbF<sub>3</sub>, CsPbF<sub>2</sub>I, and CsPbFI<sub>2</sub>.

in Fig. 6 and Fig. 7, respectively. In Fig. 6, all the sharp peaks are due to the excitonic transitions at the energy band gap edge which are allowed in the infrared spectrum. The refractive indexes  $n(0)$  and  $n(\omega)$  obtained are given in Table II. The static refractive index  $n(0)$  of CsPbF<sub>3</sub>, CsPbF<sub>2</sub>I, and CsPbFI<sub>2</sub> is found to have the value of 2.368, 1.704, and 1.735 and it reaches the maximum value of 3.054, 2.282, and 2.135, respectively.

The covalent compounds have higher values of the refractive index than ionic compounds. More electrons are shared by the ions in the covalent bonding than ionic bonding. Hence, any electrons are distributed through the structure and interact with the incident photons to slow down [32]. The refractive indices are gradually decreased in the visible and ultraviolet region. The zero-frequency reflectivity  $R(0)$  values are 0.2589, 0.2603, and 0.5014 and the frequency-dependent reflectivity  $R(\omega)$  values are 1.28, 0.55, and 0.75 for CsPbF<sub>3</sub>, CsPbF<sub>2</sub>I, and CsPbFI<sub>2</sub>, respectively.

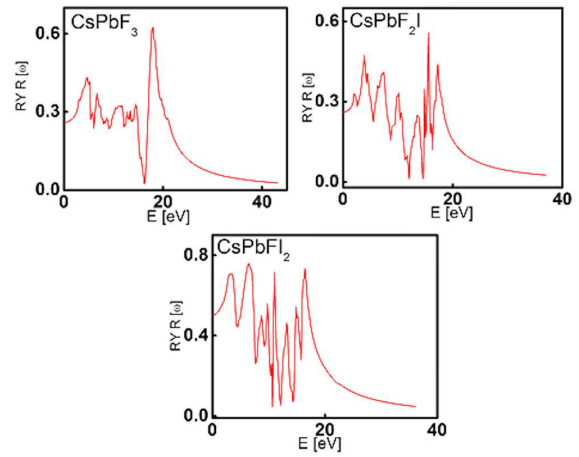


Fig. 7. Energy versus reflectivity of CsPbF<sub>3</sub>, CsPbF<sub>2</sub>I, and CsPbFI<sub>2</sub>.

The reflectivity of all these perovskites is appreciably lying in low energy regions and also describes the semiconducting behavior and further the reflectivity decreases with the increase in the photon energy and corresponds to the zero crossings of the real part of the dielectric constant.

#### 4. Conclusions

The structural properties of CsPbF<sub>3-y</sub>I<sub>y</sub> ( $y = 0, 1, 2$ ) Pb-based halide perovskites are investigated. The calculated ground state properties are in good agreement with the available theoretical results. The electronic structure reveals that these materials are semiconductors with the wide energy gap values of 2.72, 1.473, and 1.364 eV for CsPbF<sub>3</sub>, CsPbF<sub>2</sub>I, and CsPbFI<sub>2</sub>, respectively. Chemical and structural changes increase the overlap between the orbitals of Pb and F ions, which result in the shrinking of the band gap. This principle can be used to suggest practical rules for tuning the energy gap. The calculated optical parameters of these semiconducting alloys are lying in the UV range of the optical radiation and these materials can serve as promising materials for UV photodetectors, UV light emitters, and power electronic applications.

#### Acknowledgments

The support received from the college management is greatly acknowledged.

#### References

- [1] S.F. Hoefler, G. Trimmel, T. Rath, *Monatsh Chem.* **148**, 795 (2017).
- [2] G.E. Eperon, S.D. Stranks, C. Menelaou, M.B. Johnston, L.M. Herz, H.J. Snaith, *Energy Environ. Sci.* **7**, 982 (2014).
- [3] D.M. Trots, S.V. Myagkota, *J. Phys. Chem. Solids* **69**, 2520(2008).

- [4] P. Berastegui, S. Hull, S.G. Eriksson, *J. Phys. Condens. Matter* **13**, 5077 (2001).
- [5] Y. Ye, X. Run, X.H. Tao, H. Feng, X. Fei, W.L. Jun, *Chin. Phys. B* **24**, 116302 (2015).
- [6] M. Ahmad, G. Rehman, L. Ali, M. Shafiq, R. Iqbal, R. Ahmad, T. Khan, S.J. Asadabadi, M. Maqbool, *J. Alloys Compd.* **705**, 828 (2017).
- [7] G. Murtaza, I. Ahmad, M. Maqbool, H.A. Rahnamaye Aliabad, A. Afaq, *Chin. Phys. Lett.* **28**, 117803 (2011).
- [8] G. Murtaza, I. Ahmad, *Physica B* **406**, 3222 (2011).
- [9] J. Qian, B. Xu, W. Tian, *Org. Electron.* **37**, 61 (2016).
- [10] Y.H. Chang, C.H. Park, *J. Korean Phys. Soc.* **44**, 889 (2004).
- [11] J.H. Noh, S.H. Im, J.H. Heo, T.N. Mandal, S.I. Seok, *Nano Lett.* **13**, 1764 (2013).
- [12] S. Meloni, G. Palermo, N.A. Astani, M. Gratzel, U. Rothlisberger, *J. Mater. Chem.* **A4**, 159972 (2016).
- [13] Y. Wang, M.I. Dar, L.K. Ono et al., *Science* **365**, 591 (2019).
- [14] S. Kajal, G.H. Kim, C.W. Myung, Y.S. Shin, J. Kim, J. Jeong, A. Jana, J.Y. Kim, K.S. Kim, *J. Mater. Chem. A* **7**, 21740 (2019).
- [15] C. Yi, C. Liu, K. Wen et al., *Nat. Commun.* **11**, 4736 (2020).
- [16] D.B. Straus, S. Guo, A.M.M. Abeykoon, R.J. Cava, *Adv. Mater.* **32**, 2001069 (2020).
- [17] G. Roma, A. Marrognier, J. Even, *Phys. Rev. Mater.* **4**, 092402 (2020).
- [18] N. Ding, W. Xu, D. Zhou et al., *Nano Energy* **76**, 105103 (2020).
- [19] F. Ke, C. Wang, C. Jia et al., *Nat. Commun.* **12**, 461 (2021).
- [20] R. Rajeswarapalanichamy, A. Amudhavalli, R. Padmavathy, K. Iyakutti, *Mater. Sci. Eng. B* **258**, 114560 (2020).
- [21] G. Kresse, J. Hafner, *Phys. Rev. B* **47**, 558 (1993).
- [22] G. Kresse, J. Hafner, *Phys. Rev. B* **50**, 13181 (1994).
- [23] G. Kresse, J. Furthmuller, *Comput. Mater. Sci.* **6**, 15 (1996).
- [24] G. Kresse, J. Furthmuller, *Phys. Rev. B* **54**, 11169 (1996).
- [25] G. Kresse, D. Joubert, *Phys. Rev. B* **59**, 1758 (1999).
- [26] J.P. Perdew, Y. Wang, *Phys. Rev. B* **45**, 13244 (1992).
- [27] H.J. Monkhorst, J.D. Pack, *Phys. Rev. B* **13**, 5182 (1976).
- [28] O.K. Anderson, *Phys. Rev. B* **12**, 3060 (1975).
- [29] S.Q. Wu, Z.F. Hou, Z.Z. Zhu, *Solid State Commun.* **143** 425 (2007).
- [30] H.A. Kramers, in: *Transactions of Volta Centenary Congress, Atti Congr. Int. Fis.* **2**, 545 (1927).
- [31] R. de L. Kronig, *J. Opt. Soc. Am.* **12**, 547 (1926).
- [32] K.E. Babu, A. Veeraiah, D.T. Swamy, V. Veeraiah, *Mater. Sci.-Poland* **30**, 359 (2012).